Ovarian Teratomas: Tumor Types and Imaging Characteristics[1]

Eric K. Outwater, MD • Evan S. Siegelman, MD • Jennifer L. Hunt, MD

CME FEATURE

See accompanying test at http://www.rsna.org/education/rg_cme.html

LEARNING OBJECTIVES FOR TEST 6

After reading this article and taking the test, the reader will be able to:

- Enumerate the most common types of ovarian teratomas.
- Discuss the histologic characteristics and specific US, CT, and MR imaging features of the various types of ovarian teratomas.
- Differentiate between mature cystic teratomas, immature teratomas, and monodermal teratomas on the basis of histologic and radiologic findings.

Ovarian teratomas include mature cystic teratomas (dermoid cysts), immature teratomas, and monodermal teratomas (eg, struma ovarii, carcinoid tumors, neural tumors). Most mature cystic teratomas can be diagnosed at ultrasonography (US) but may have a variety of appearances, characterized by echogenic sebaceous material and calcification. At computed tomography (CT), fat attenuation within a cyst is diagnostic. At magnetic resonance (MR) imaging, the sebaceous component is specifically identified with fat-saturation techniques. The US appearances of immature teratoma are nonspecific, although the tumors are typically heterogeneous, partially solid lesions, usually with scattered calcifications. At CT and MR imaging, immature teratomas characteristically have a large, irregular solid component containing coarse calcifications. Small foci of fat help identify these tumors. The US features of struma ovarii are also nonspecific, but a heterogeneous, predominantly solid mass may be seen. On T1- and T2-weighted images, the cystic spaces demonstrate both high and low signal intensity. Familiarity with the US, CT, and MR imaging features of ovarian teratomas can aid in differentiation and diagnosis.

Abbreviation: H-E = hematoxylin-eosin

Index terms: Dermoid, 852.313 • Ovary, cysts, 852.313 • Ovary, neoplasms, 852.313 • Teratoma, 852.313

RadioGraphics 2001; 21:475–490

[1] From the Department of Radiology, University of Arizona, 1501 N Campbell Ave, Rm 1361, Tucson, AZ 85724-5067 (E.K.O.); and the Departments of Radiology (E.S.S.) and Pathology (J.L.H.), University of Pennsylvania, Philadelphia. Received March 30, 2000; revision requested May 30 and received July 5; accepted July 6. **Address correspondence to** E.K.O. (e-mail: *outwater@radiology.arizona.edu*).

Introduction

Ovarian teratomas are the most common germ cell neoplasm and, in many series, the most common excised ovarian neoplasm. Teratomas comprise a number of histologic types of tumors, all of which contain mature or immature tissues of germ cell (pluripotential) origin. The most common of these tumors, the mature cystic teratoma (also known as dermoid cyst), typically contains mature tissues of ectodermal (skin, brain), mesodermal (muscle, fat), and endodermal (mucinous or ciliated epithelium) origin. In monodermal teratomas, one of these tissue types (eg, thyroid tissue in struma ovarii, neuroectodermal tissue in carcinoid tumor) predominates.

Although the typical imaging manifestations of mature cystic teratomas are well described, the less common types of ovarian teratomas (eg, immature teratomas, monodermal teratomas) have received less attention in the imaging literature. Consequently, we sought to review the full spectrum of imaging findings in ovarian teratomas. Recent studies of these tumors with magnetic resonance (MR) imaging have suggested that this modality may demonstrate specific features of teratomas (1–5). In this article, we discuss and illustrate typical manifestations of mature cystic teratomas (dermoid cysts), immature teratomas, and monodermal teratomas of the ovary (struma ovarii, carcinoid tumors, neural tumors) at computed tomography (CT), ultrasonography (US), and MR imaging.

Mature Cystic Teratomas (Dermoid Cysts)

Mature cystic teratomas (a more appropriate term than the commonly used "dermoid cysts") are cystic tumors composed of well-differentiated derivations from at least two of the three germ cell layers (ectoderm, mesoderm, and endoderm). They affect a younger age group (mean patient age, 30 years) than epithelial ovarian neoplasms (6). Mature cystic teratoma is the most common germ cell neoplasm and, in some series, the most common ovarian neoplasm removed at surgery (7,8). It is the most common ovarian mass in children (9). Mature cystic teratomas arise from a single germ cell after the first meiotic division (10). Most mature cystic teratomas are asymptomatic. Abdominal pain or other nonspecific symptoms occur in the minority of patients (6). Mature cystic teratomas grow slowly at an average rate of 1.8 mm each year, prompting some investigators to advocate nonsurgical management of smaller (<6-cm) tumors (11). Mature cystic teratomas requiring removal can be treated with simple cystectomy. The tumors are bilateral in about 10% of cases (12).

The gross pathologic appearance of mature cystic teratomas is characteristic. The tumors are unilocular in 88% of cases and are filled with sebaceous material, which is liquid at body temperature and semisolid at room temperature (Fig 1) (12). Squamous epithelium lines the wall of the cyst, and compressed, often hyalinized ovarian stroma covers the external surface (Fig 1) (13,14). Hair follicles, skin glands, muscle, and other tissues lie within the wall. There is usually a raised protuberance projecting into the cyst cavity known as the Rokitansky nodule. Most of the hair typically arises from this protuberance. When bone or teeth are present, they tend to be located within this nodule (Fig 2) (15). Ectodermal tissue (skin derivatives and neural tissue) is invariably present (12,13,15). Mesodermal tissue (fat, bone, cartilage, muscle) is present in over 90% of cases, and endodermal tissue (eg, gastrointestinal and bronchial epithelium, thyroid tissue) is seen in the majority of cases (Fig 3) (12). Adipose tissue is present in 67%–75% of cases, and teeth are seen in 31% (12,13,15).

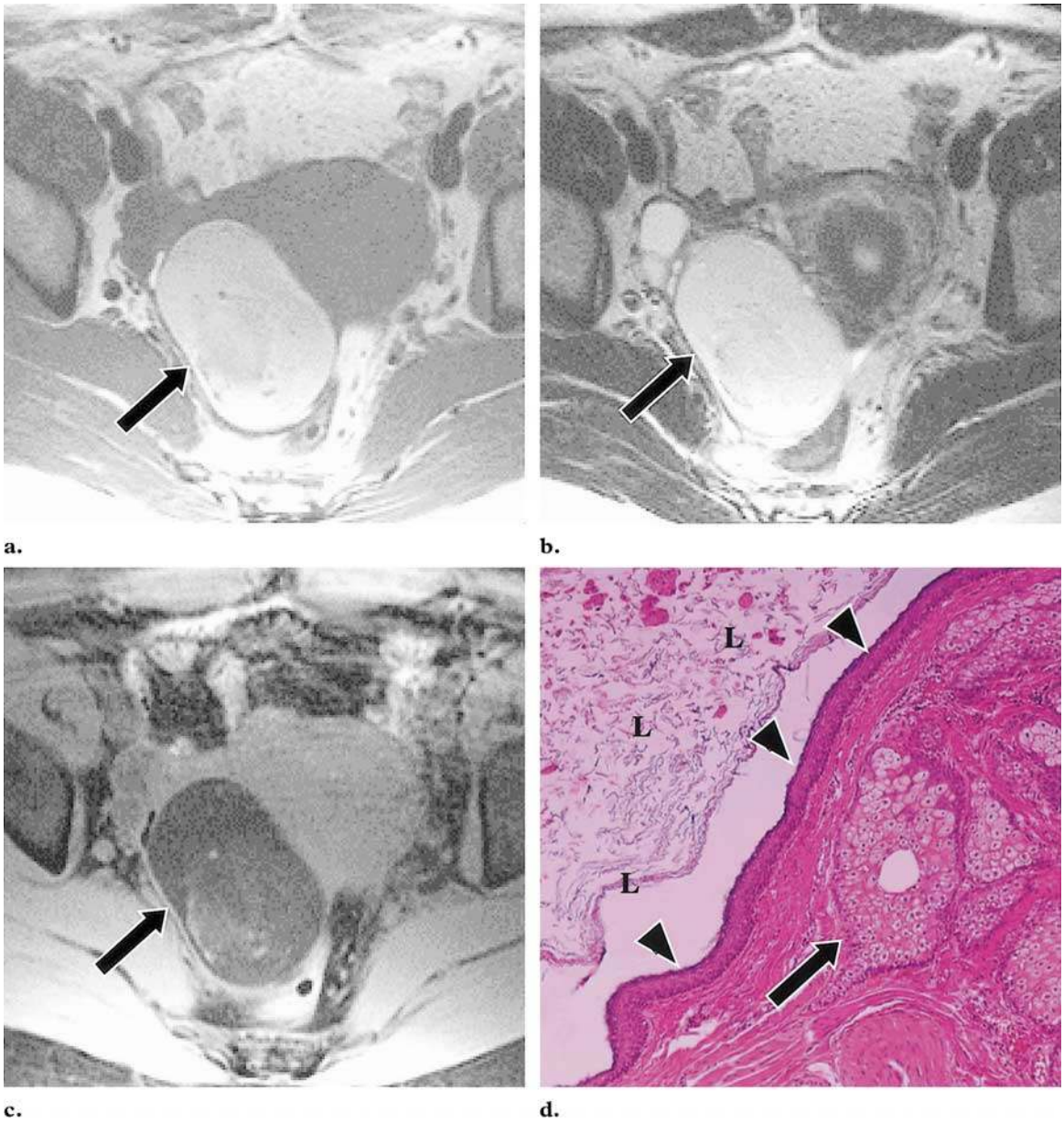

Figure 1. Mature cystic teratoma in a 48-year-old woman. **(a)** Axial T1-weighted spin-echo MR image (repetition time msec/echo time msec = 879/14) shows a high-signal-intensity mass of the right ovary (arrow). **(b)** On a T2-weighted fast spin-echo MR image (4,050/105 [effective]), the mass demonstrates heterogeneous internal signal intensity with punctate high signal intensity (arrow). **(c)** Axial fat-saturated T1-weighted gradient-echo MR image (290/2.1) demonstrates saturation of the cyst contents (arrow). **(d)** Photomicrograph (original magnification, ×40; hematoxylin-eosin [H-E] stain) of the cyst wall shows squamous cell lining (arrowheads), sebaceous glands (arrow), and intervening muscle. Sebaceous material and cell debris are seen filling the cyst lumen (*L*).

Figure 2. Mature cystic teratoma in a 20-year-old woman. **(a)** Sagittal US image demonstrates a mostly echogenic mass (arrows) with some sound attenuation. **(b)** On an axial contrast material–enhanced CT scan, the cyst cavity demonstrates fat attenuation (*F*). A round Rokitansky nodule is seen (arrow) and has a feathery appearance at the fatty interface where the hair arises from it (arrowhead). **(c)** Photograph of the bisected tumor shows the two components of the fat attenuation seen in **b**: the Rokitansky nodule (thick arrow), which has the yellowish appearance of adipose tissue, and sebaceous components (*F*). Teeth are seen in the center of the Rokitansky nodule and account for the calcification seen in **b**. The bulk of the cyst cavity is filled with hair (arrowheads). Note how the cyst wall is folded back (thin arrow).

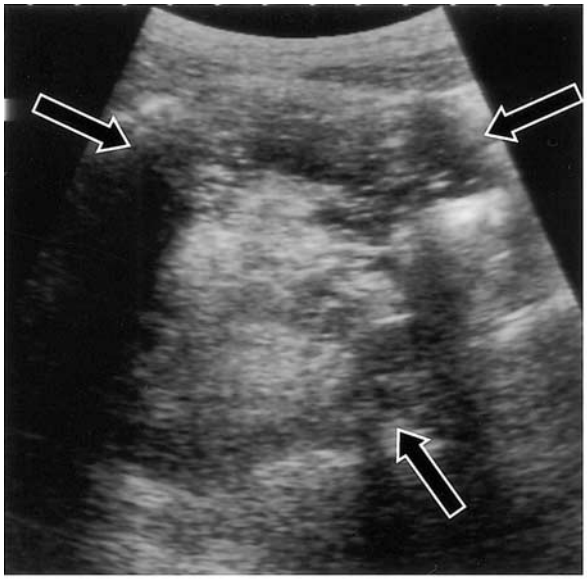

a.

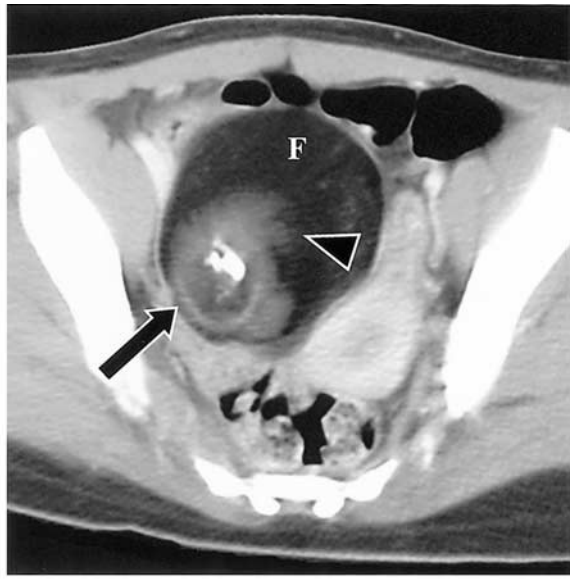

b.

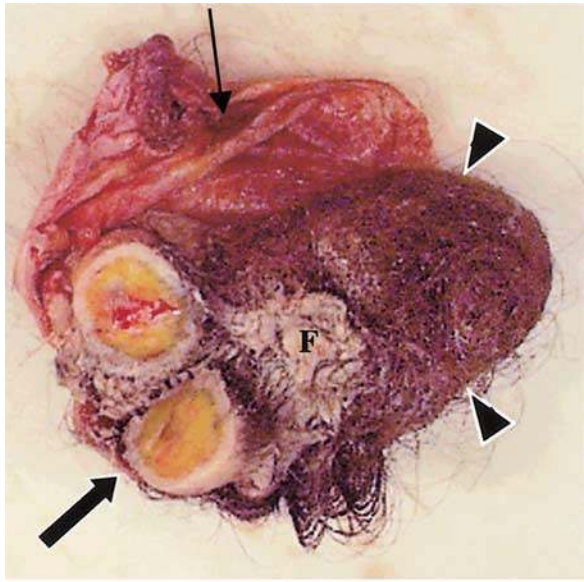

c.

Most mature cystic teratomas can be diagnosed at US. However, the US diagnosis is complicated by the fact that these tumors may have a variety of appearances. Three manifestations occur most commonly. The most common manifestation is a cystic lesion with a densely echogenic tubercle (Rokitansky nodule) projecting into the cyst lumen (16). The second manifestation is a diffusely or partially echogenic mass with the echogenic area usually demonstrating sound attenuation owing to sebaceous material and hair within the cyst cavity (Fig 4) (17,18). The third manifestation consists of multiple thin, echogenic bands caused by hair in the cyst cavity (Fig 3). Pure sebum within the cyst may be hypoechoic or anechoic (19). Fluid-fluid levels result from sebum floating above aqueous fluid, which appears more echogenic than the sebum layer (18). The dermoid plug is echogenic, with shadowing due to adipose tissue or calcifications within the plug or to hair arising from it. Diffuse echogenicity in these tumors is caused by hair mixed with the cyst fluid (Fig 4).

Figure 3. Mature cystic teratoma of the ovary without intracystic lipid material in a 31-year-old woman. **(a)** Transabdominal US image shows a heterogeneous mass containing echogenic reflectors representing hair. There is no evidence of calcification or fat. **(b)** Axial T1-weighted spin-echo MR image (683/16) shows a high-signal-intensity nodule in the wall of the mass. **(c)** Axial fat-saturated T1-weighted gradient-echo MR image (330/2.9) demonstrates saturation of the fatty nodule (arrow). **(d)** Photomicrograph (original magnification, ×40; H-E stain) shows adipose tissue within the fatty nodule.

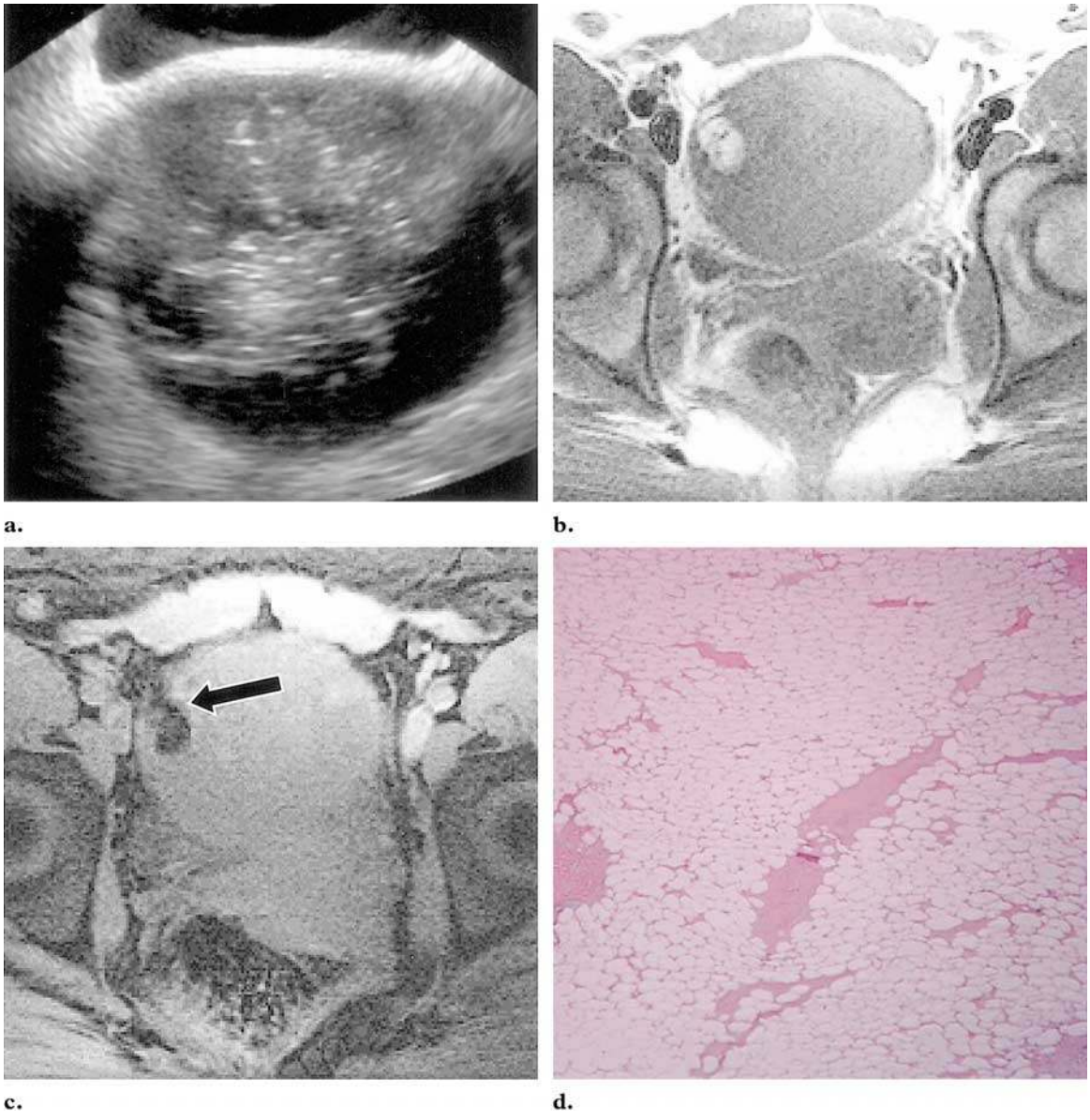

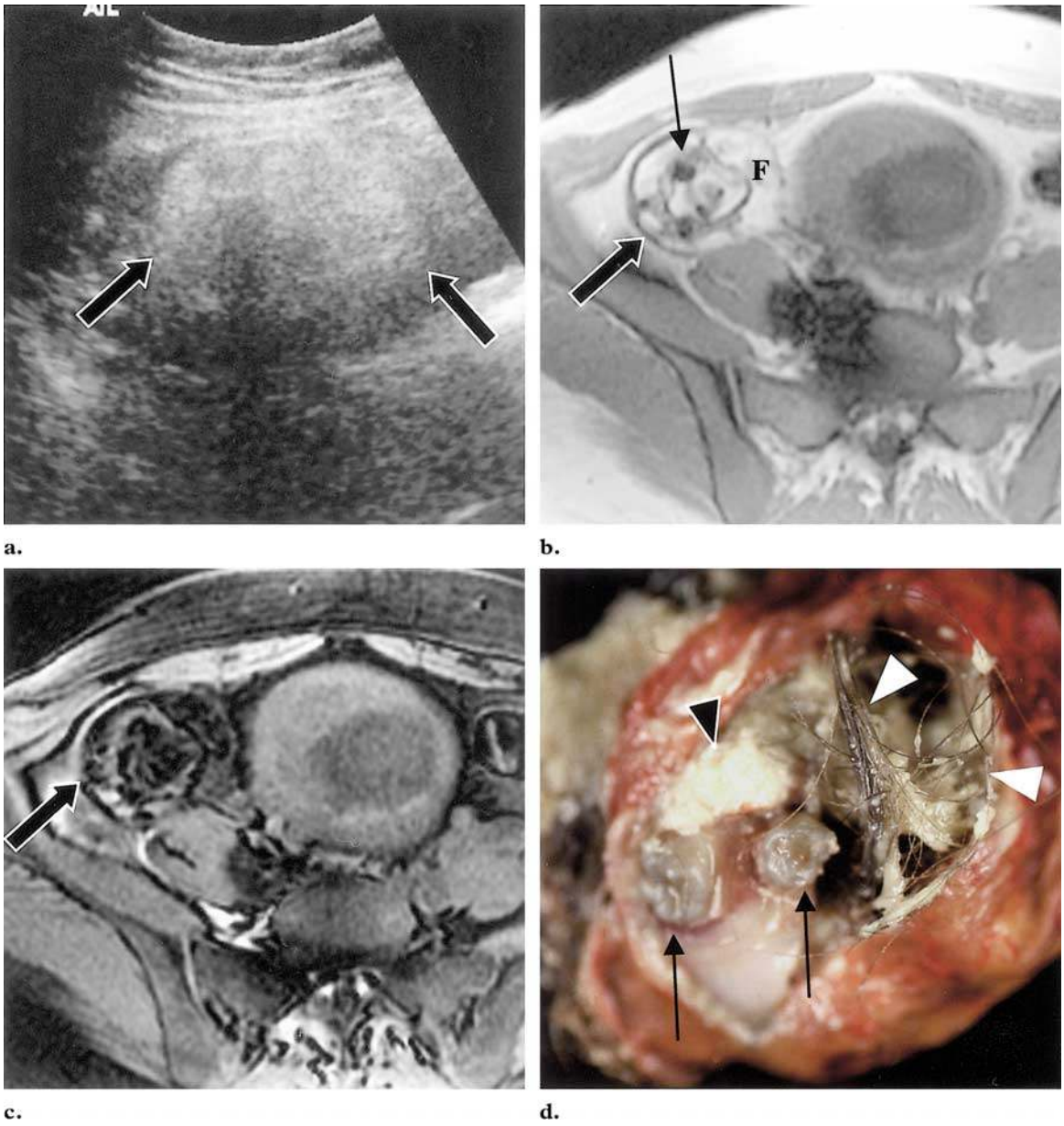

Figure 4. Mature cystic teratoma of the right ovary in a 19-year-old pregnant woman. **(a)** Sagittal transabdominal US image shows an echogenic mass with sound attenuation (arrows). **(b)** T1-weighted gradient-echo MR image (200/4.2) shows the mass (thick arrow) with high-signal-intensity fat (*F*). Low-signal-intensity central calcifications are also seen (thin arrow). **(c)** On a fat-suppressed T1-weighted gradient-echo MR image (200/2.1), the signal of the lipid material within the mass is suppressed (arrow). **(d)** Photograph of the gross specimen shows yellowish, pasty sebaceous material (black arrowhead) and hair (white arrowheads) within the cyst cavity, findings that account for the fat echogenicity and signal intensity seen at US and MR imaging. Two molar teeth are also evident (arrows).

In a prospective US study that made use of these criteria, Mais et al (20) found a sensitivity of 58% and a specificity of 99% in the diagnosis of mature cystic teratoma. Numerous pitfalls have been described in the US diagnosis of mature cystic teratoma (21). Blood clot within a hemorrhagic cyst can appear echogenic, although a mature cystic teratoma usually demonstrates sound attenuation rather than increased through-transmission. Hemorrhagic cysts or blood clots typically demonstrate increased through-transmission. Echogenic bowel can frequently be mistaken for diffusely echogenic mature cystic teratoma and vice versa (21). Perforated appendix with appendicolith and fibrous lesions such as cystadenofibromas have also been described as false-positive findings (21,22).

The diagnosis of mature cystic teratoma at CT and MR imaging is fairly straightforward because these modalities are more sensitive for fat (23). At CT, fat attenuation within a cyst, with or without calcification in the wall, is diagnostic for mature cystic teratoma (19,24,25). A floating mass of hair can sometimes be identified at the fat–aqueous fluid interface (19,24). Fat is reported in 93% of cases and teeth or other calcifications in 56% (25).

At MR imaging, the sebaceous component of dermoid cysts has very high signal intensity on T1-weighted images, similar to retroperitoneal fat. The signal intensity of the sebaceous component on T2-weighted images is variable, usually approximating that of fat (26). This combination of different signal intensities on T1- and T2-weighted images is not specific for fat and must be distinguished from MR imaging findings in intracystic hemorrhage, which can cause shortened T1 and T2 of the cyst fluid (27–32). The imaging appearance on T1- and T2-weighted images is therefore mimicked by some hemorrhagic lesions, most prominently endometriomas.

Three methods can be used to distinguish the fatty contents of a mature cystic teratoma from endometriomas or other hemorrhagic cysts. Chemical-shift artifact in the frequency-encoding direction can be used to detect fat and distinguish it from hemorrhage (26). Gradient-echo imaging with an echo time in which fat and water are in opposite phase can demonstrate fat-water interfaces and mixtures of fat and water (33). Sequences with frequency-selective fat saturation will suppress the high signal of teratomas and help distinguish them from hemorrhagic lesions (Fig 5). MR imaging with this technique allows accurate differentiation between teratomas and hemorrhagic cysts and is preferable to the techniques described earlier (27–32). On the other hand, short-inversion-time inversion recovery sequences are not chemical shift–specific and therefore should not be relied on to distinguish hemorrhagic from fatty masses.

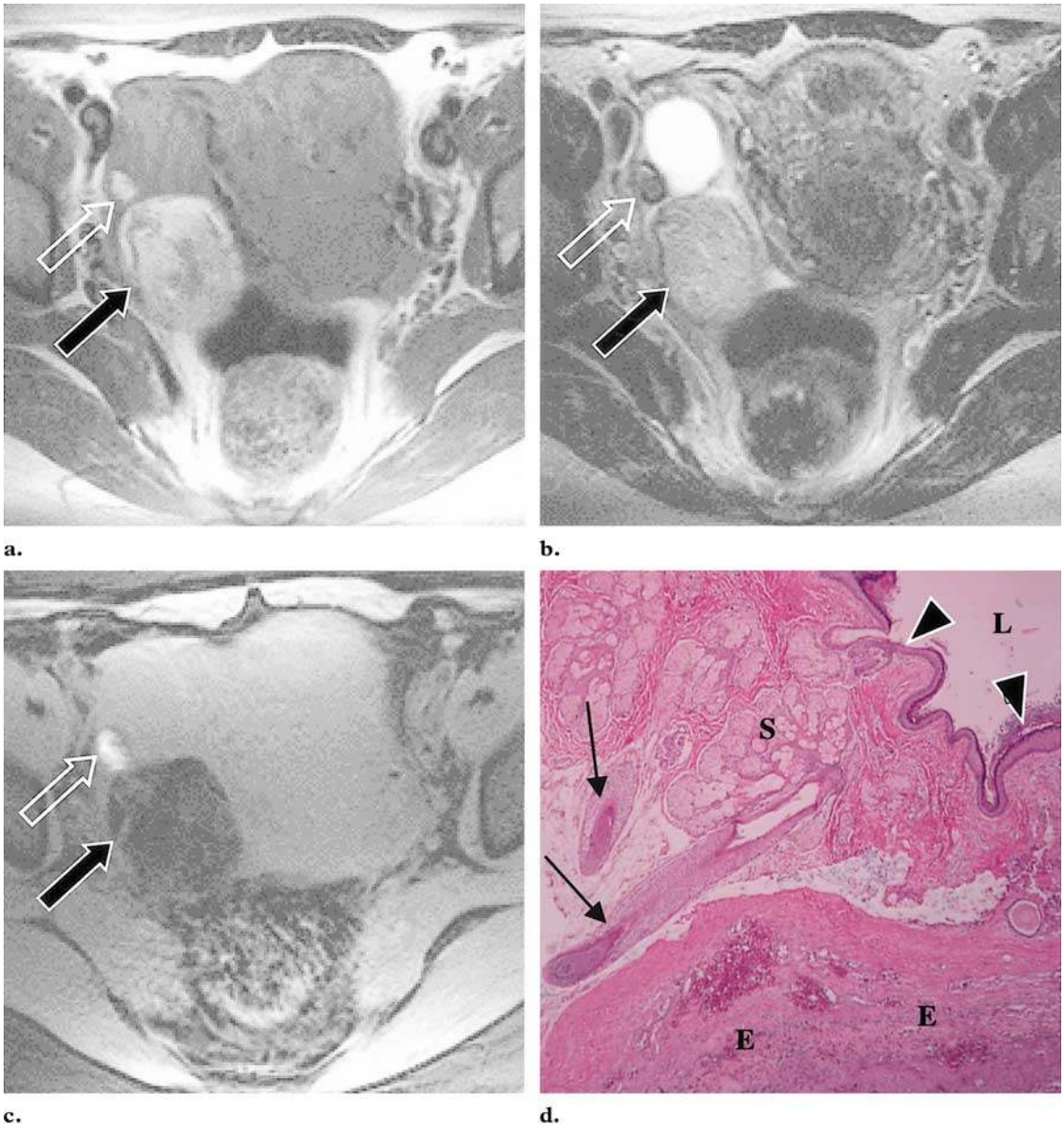

Figure 5. Mature cystic teratoma in a 51-year-old woman with endometriosis. **(a)** Axial T1-weighted spin-echo MR image (600/16) shows two high-signal-intensity masses of the right ovary (arrows). **(b)** T2-weighted fast spin-echo MR image (6,000/126 [effective]) shows the larger mass with heterogeneous internal signal intensity and punctate high signal intensity (solid arrow). The smaller mass demonstrates low-signal-intensity "shading" (open arrow), a finding that is typical of endometrioma. **(c)** Axial fat-saturated T1-weighted gradient-echo MR image (300/2.9) demonstrates saturation of the contents of the larger cyst (solid arrow). The hemorrhagic endometriosis (open arrow) still has high signal intensity. (**d**) Photomicrograph (original magnification, ×40; H-E stain) of the cyst wall shows squamous cells (arrowheads) lining the cyst lumen (*L*) as well as sebaceous glands (*S*) and hair follicles (arrows). Adjacent endometriosis (*E*) is indicated by the presence of fibrosis and hemorrhage.

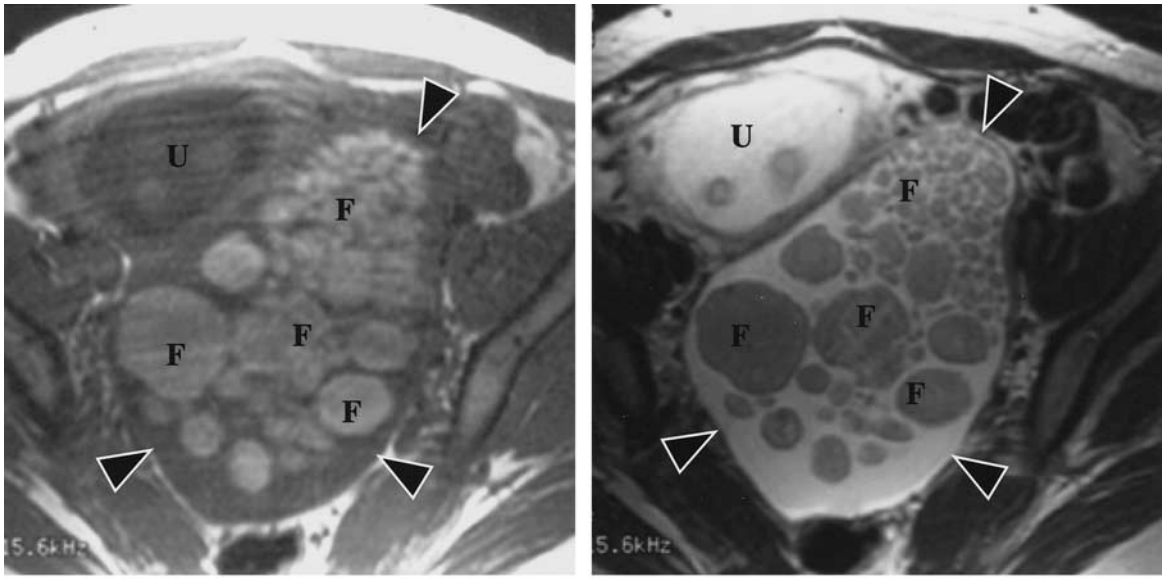

Figure 6. Dermoid cyst and intracystic nondependent spheres of lipid material in a 24-year-old pregnant woman. *U* = uterus. **(a)** T1-weighted MR image (783/8) shows a large cyst (arrowheads) containing multiple round masses (*F*). **(b)** T2-weighted MR image (7,533/84 [effective]) shows the round masses (*F*) floating in high-signal-intensity fluid within the cyst (arrowheads). **(c)** Fat-saturated T1-weighted MR image (666/8) shows the masses with slightly diminished signal intensity (*F*) compared with the non–fat-saturated T1-weighted image (cf **a**). (Courtesy of R. Epstein, MD, Department of Radiology, University of Medicine and Dentistry of New Jersey, New Brunswick).

A minority of mature cystic teratomas will not demonstrate a sebum-filled cyst cavity (24). However, these teratomas usually demonstrate evidence of fat in the wall or in the Rokitansky nodule (Fig 3) (5,34). Yamashita et al (34) reported detecting such small foci of fat (but no sebaceous material) with opposed-phase imaging in seven of 78 mature cystic teratomas. No fatty tissue or sebaceous material was identified at MR imaging in five of the 78 lesions. In addition, intracystic nondependent spheres of lipid material can occasionally be identified in a mature cystic teratoma, producing a striking appearance (Fig 6) (35).

Mature cystic teratoma can be associated with complications from rupture, malignant degeneration, or (most commonly) torsion. Mature cystic teratomas affected by torsion are larger than average (mean diameter, 11 cm versus 6 cm); this enlargement could be the result of the torsion rather than the cause of it (6). Torsion of a teratoma, even in chronic cases, does not eradicate the fatty elements (Fig 7). Findings suggestive of torsion include deviation of the uterus to the twisted side, engorged blood vessels on the twisted side, a mass with a high-signal-intensity rim on T1-weighted MR images, a low-signal-intensity torsion knot, and thick, straight blood vessels that drape around the mass and cause complete absence of enhancement (36,37).

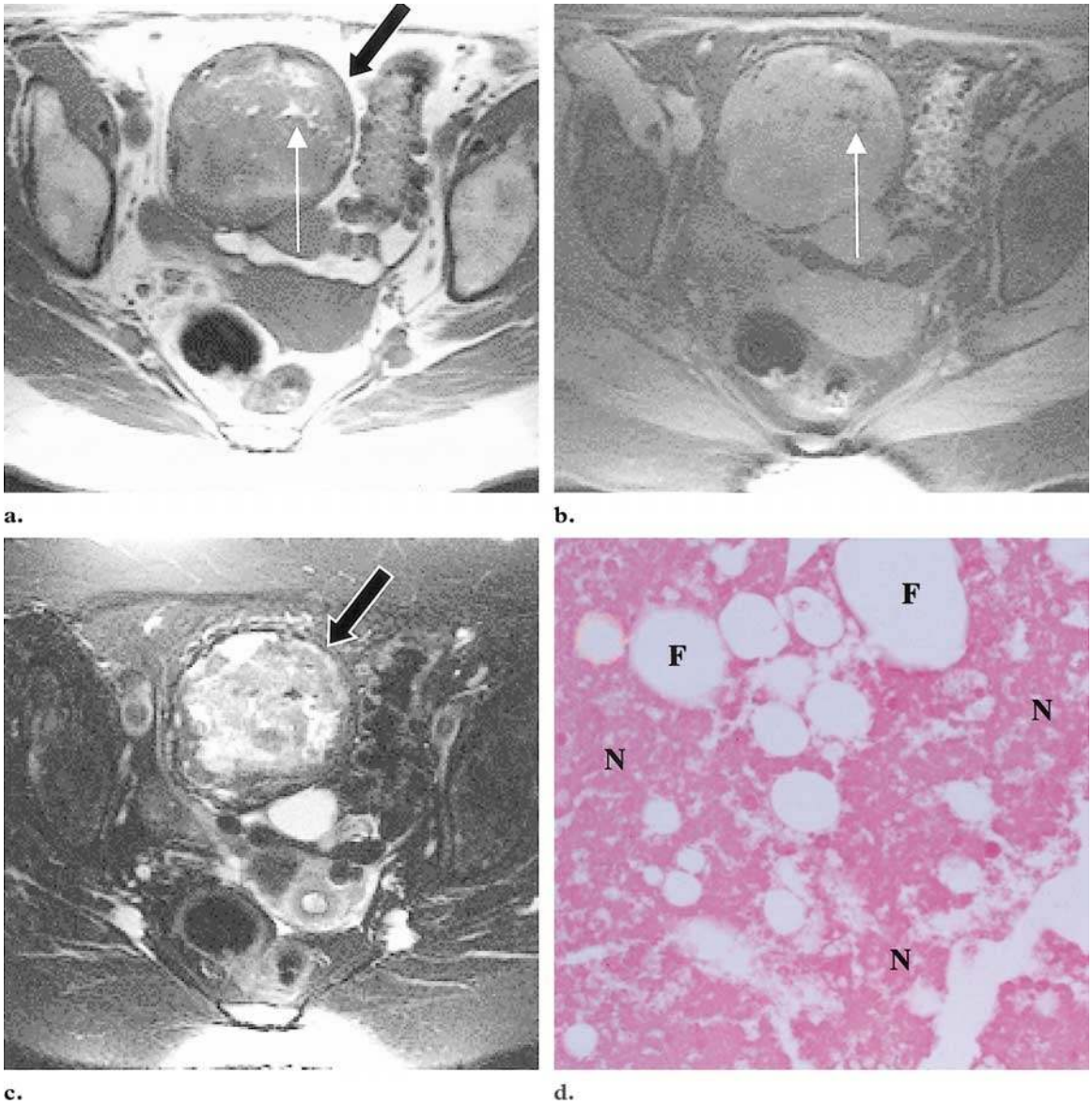

Figure 7. Infarcted mature cystic teratoma resulting from ovarian torsion in a 73-year-old woman. **(a)** Axial T1-weighted spin-echo MR image (500/8) shows a heterogeneous mass (black arrow) with high-signal-intensity foci (white arrow). **(b)** Axial fat-saturated T1-weighted gradient-echo MR image (150/1.7) demonstrates saturation of the high-signal-intensity foci within the mass (arrow), a finding that indicates fat. **(c)** Axial T2-weighted MR image (5,200/98 [effective]) shows the mass with a solid appearance (arrow). **(d)** Photomicrograph (original magnification, ×40; H-E stain) shows complete necrosis (*N*) of the teratoma, but with preservation of the fat globules (*F*).

The tumors can rupture, causing leakage of the liquefied sebaceous contents into the peritoneum and resulting in granulomatous peritonitis. However, this is a rare complication, occurring in less than 1% of cases (6).

Malignant degeneration of mature cystic teratomas consists of differentiated tissues giving rise to carcinoma or sarcoma. In contrast, immature teratomas are not known to arise from mature cystic teratomas; thus, the term *malignant transformation* applies only to malignancy arising de novo in a preexisting benign mature cystic teratoma. Squamous cell carcinoma arising from the squamous lining of the cyst is the most common type of malignant degeneration, accounting for over 80% of cases. Malignant transformation of mature cystic teratoma is a rare complication, reported to occur in 1%–2% of cases in the older literature (15). More recently, Comerci et al (6) found malignant transformation in only one of 517 cases. In contrast to mature cystic teratoma, malignant transformation occurs in the 6th or 7th decade of life. It has an imaging appearance that indicates the presence of the underlying mature cystic teratoma: a sebaceous lipid component as well as a heterogeneous solid component protruding into the cavity or extending transmurally into adjacent organs (1,25).

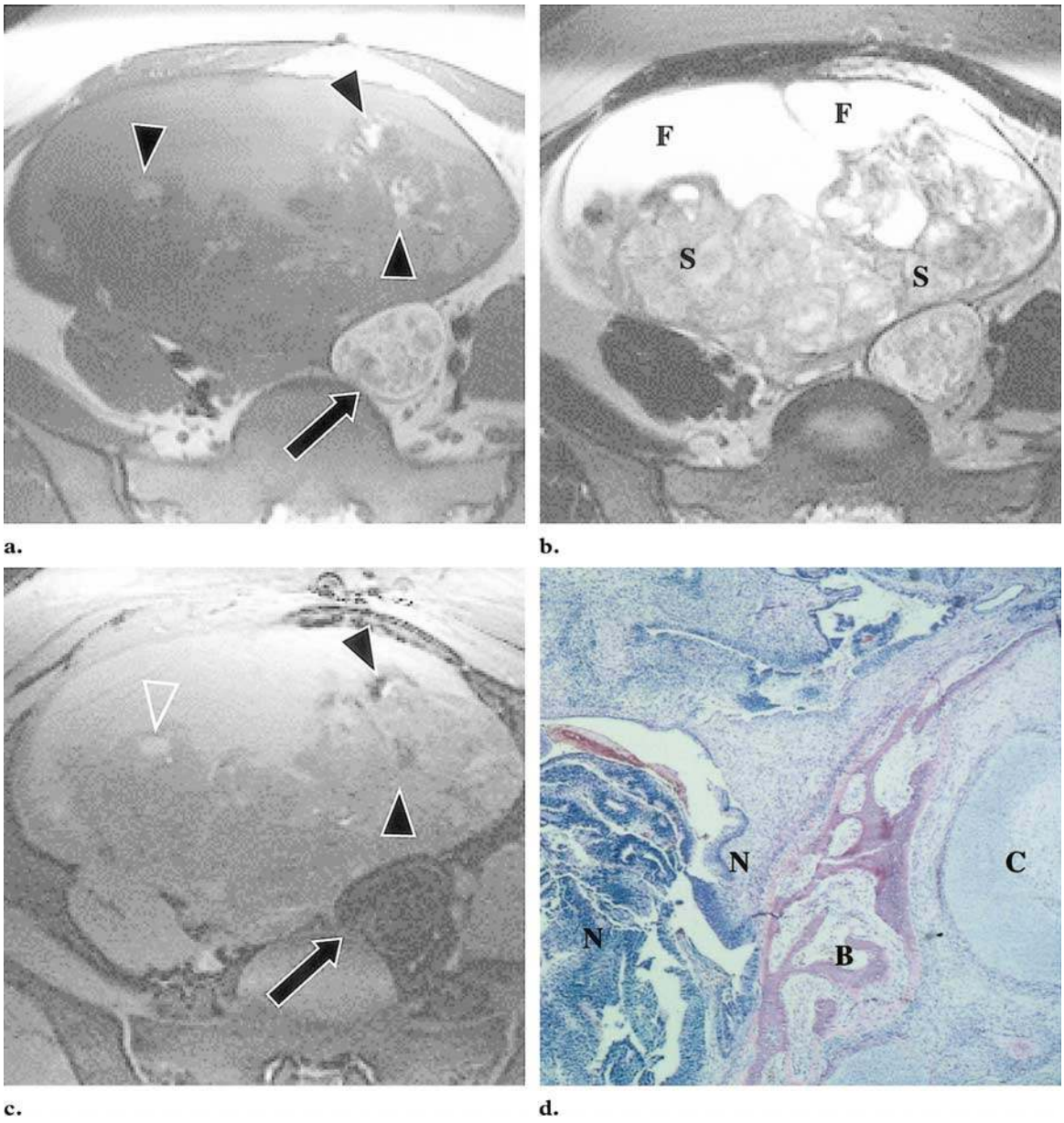

Figure 8. Immature teratoma associated with ipsilateral mature cystic teratoma in a 27-year-old woman. **(a)** Axial T1-weighted spin-echo MR image (500/11) shows a large mass of the left ovary with multiple high-signal-intensity foci (arrowheads). A lesion with the typical appearance of a mature cystic teratoma lies adjacent to the mass (arrow). **(b)** Axial T2-weighted fast spin-echo MR image (3,000/126 [effective]) shows the large fluid (*F*) and solid (*S*) components of the mass. **(c)** Fat-suppressed T1-weighted fast multiplanar spoiled gradient-echo MR image (200/3.6) shows that some of the high-signal-intensity foci in **a** are hemorrhagic and retain their high signal intensity (open arrowhead), whereas others represent foci of fat (solid arrowheads). The ipsilateral mature cystic teratoma demonstrates suppression of the signal of the cyst contents (arrow). **(d)** Photomicrograph (original magnification, ×40; H-E stain) of the large mass shows immature neural tissue (*N*), bone (*B*), and cartilage (*C*).

Immature Teratomas

Like mature cystic teratomas, immature teratomas are composed of tissues derived from the three germ layers. Immature teratomas differ from mature cystic teratomas in that they demonstrate clinically malignant behavior, are much less common (<1% of ovarian teratomas), affect a younger age group (usually during the first 2 decades of life), and are histologically distinguished by the presence of immature or embryonic tissues (Fig 8) (14).

At initial manifestation, immature teratomas are typically larger (14–25 cm) than mature cystic teratomas (average, 7 cm) (12,38). They may be solid or have a prominent solid component with cystic elements (39). The cystic areas are usually filled with serous or mucinous fluid or may be filled with fatty sebaceous material. The tumors frequently demonstrate perforation of the capsule, which is not always well defined (14). Mature tissue elements similar to those seen in

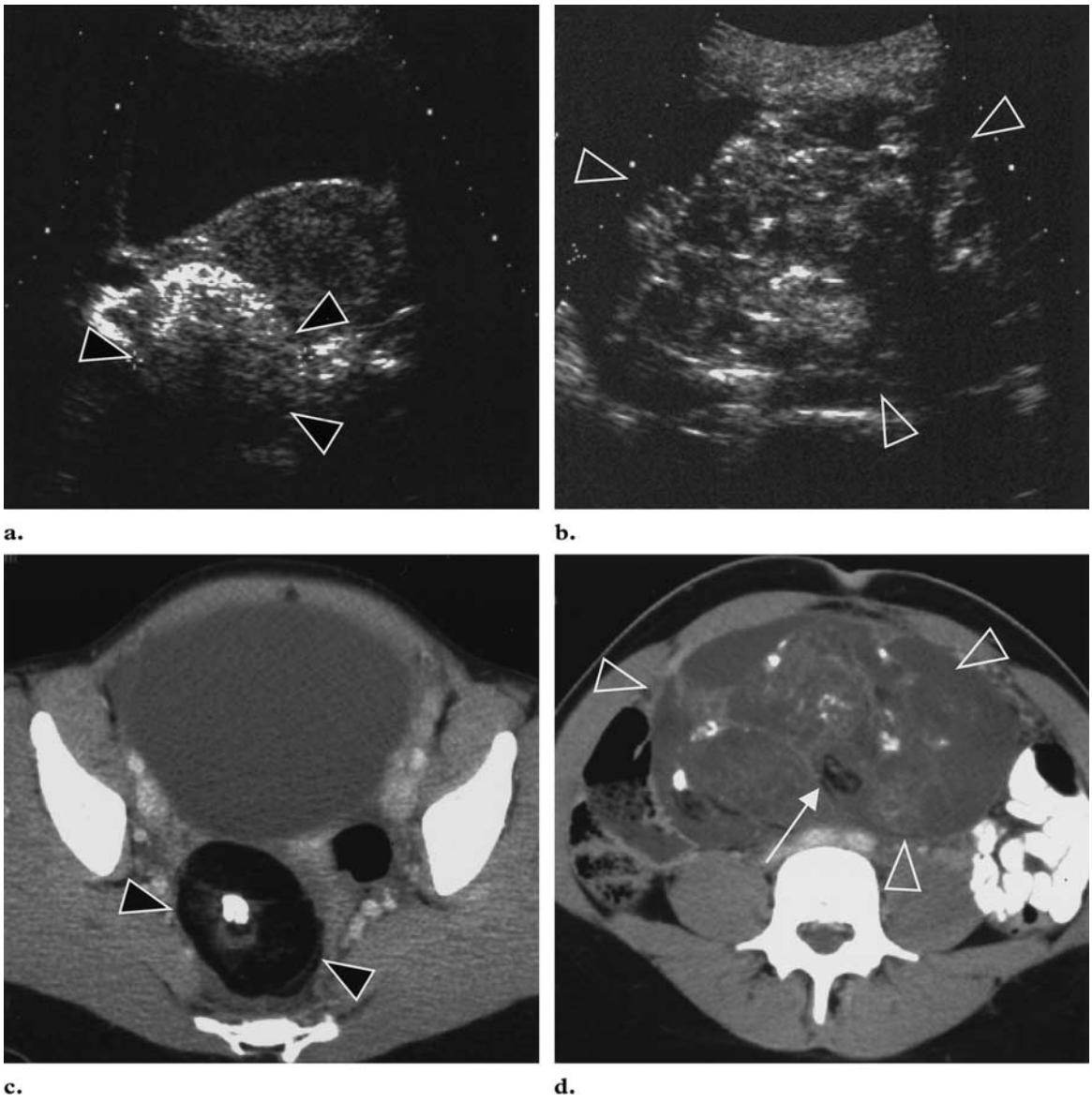

Figure 9. Immature teratoma associated with contralateral mature cystic teratoma in a 27-year-old woman. The patient's α-fetoprotein level was 571 μg/L (normal, <15 μg/L). **(a)** Transverse transabdominal US image shows a heterogenous mass in the cul-de-sac (arrowheads). **(b)** Transverse transabdominal US image through the midabdomen shows a larger mass containing calcifications (arrowheads). Foci of fat are difficult to appreciate. **(c)** CT scan through the pelvis shows a mature cystic teratoma in the cul-de-sac with fat attenuation and central calcification (arrowheads). **(d)** CT scan through the abdominal mass shows an immature teratoma (arrowheads) with foci of fat (arrow) and scattered calcifications.

mature cystic teratoma are invariably present. Tumor grading is based on the amount of immature tissue present. Recently, the amount of yolk sac tumor within immature teratomas has been recognized as both the source of α-fetoprotein in affected patients and the major predictor of stage, grade, and rate of recurrence (40). Surgical treatment is usually curative for stage I lesions (41).

Immature teratomas are associated with mature cystic teratomas (Fig 8). Ipsilateral typical mature cystic teratomas are present in 26% of cases of immature teratoma, and an immature teratoma will be seen in the contralateral ovary in 10% (Fig 9) (42). Immature teratomas, which are treated with chemotherapy, can undergo tissue maturation and take on an appearance more typical of mature cystic teratoma, a phenomenon known as retroconversion (43). These retroconverted masses can remain stable for a long period of time (43,44).

The US appearances of immature teratoma are nonspecific (45). Typically, the tumors are heterogeneous, partially solid lesions (46,47). Scattered calcifications are usually present. Small foci of fat within the solid component may be difficult to recognize. At CT and MR imaging, these tumors have a characteristic appearance (46,47). A large, irregular solid component containing coarse calcifications and small foci of fat is seen (25,46–48). Hemorrhage is often present.

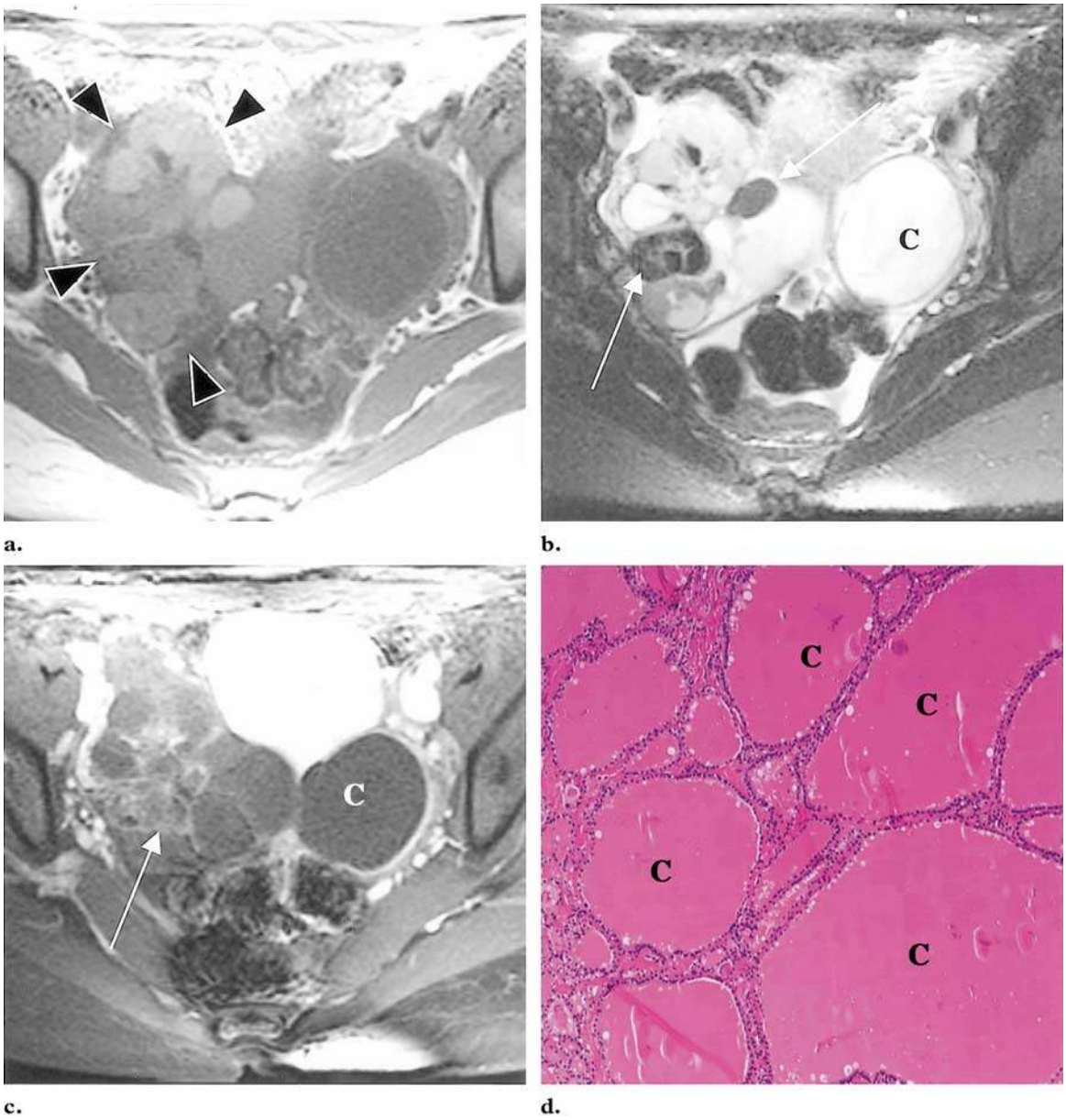

Figure 10. **(a–c)** Struma ovarii in a 35-year-old woman. **(a)** Axial T1-weighted spin-echo MR image (500/8) shows a mass of the right ovary with multiple loculations (arrowheads), some of which have high signal intensity. **(b)** T2-weighted fast spin-echo MR image (6,000/105 [effective]) shows some of the cyst loculations with very low signal intensity (arrows). *C* = functional cyst. **(c)** Axial gadolinium-enhanced fat-saturated T1-weighted gradient-echo MR image (180/1.7) shows the loculations with lacelike enhancement (arrow). *C* = functional cyst. **(d)** Struma ovarii. Photomicrograph (original magnification, ×40; H-E stain) of a specimen from a different patient shows thyroid follicles containing thick colloid (*C*).

Although smaller mature teratomas may occur, they are uncommon.

Another type of teratoma, the mature solid teratoma, has also been described. This tumor is mostly solid but has no identifiable immature components and therefore does not meet the criteria for an immature teratoma. It must be extensively sampled at biopsy to exclude an immature teratoma (49). Unlike immature teratomas, mature solid teratomas are benign, corresponding to grade 0 immature teratomas. They are radiologically indistinguishable from immature teratomas and occur in a similar age group. Fat may be visible at MR imaging or CT (4).

Monodermal Teratomas

Monodermal teratomas are composed predominantly or solely of one tissue type. There are three main types of ovarian monodermal tumors: struma ovarii, ovarian carcinoid tumors, and tumors with neural differentiation.

Struma Ovarii

Struma ovarii is composed predominantly or solely of mature thyroid tissue that demonstrates acini filled with thyroid colloid (Fig 10). Such thyroid tissue can occur as a minor component of

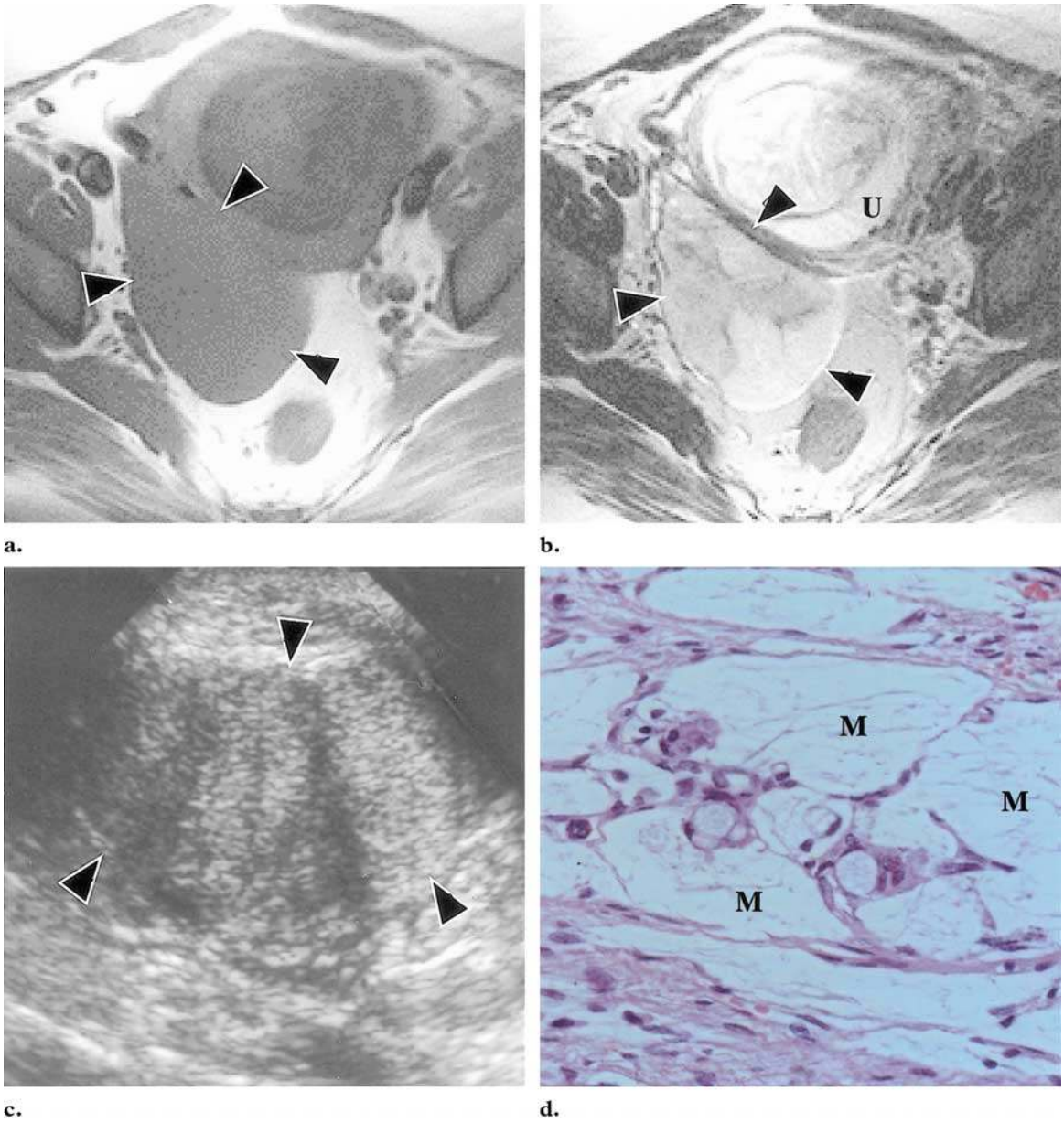

Figure 11. Monodermal teratoma (mucinous carcinoid tumor) in a 36-year-old pregnant woman. **(a)** Axial T1-weighted spin-echo MR image (897/16) shows a mass of the right ovary (arrowheads). **(b)** T2-weighted fast spin-echo MR image (4,000/119 [effective]) shows the mass with very high signal intensity due to its mucinous contents (arrowheads). *U* = uterus. **(c)** On a sagittal US image, the mass has a solid appearance (arrowheads), but there is no evidence of fat. **(d)** High-power photomicrograph (original magnification, ×100; H-E stain) of the mass shows extensive mucin (*M*) surrounding carcinoid tumor cells.

mature cystic teratomas, but in struma ovarii it is the predominant or sole tissue type. Struma ovarii accounts for approximately 3% of all mature teratomas. In rare cases, thyrotoxicosis has been seen as a complication of struma ovarii (50).

The gross pathologic appearance of struma ovarii is very different from that of mature cystic teratoma and consists of amber-colored thyroid tissue, hemorrhage, necrosis, and fibrosis. Malignancy is uncommon, and in many cases in which malignancy was diagnosed on the basis of histologic criteria, the clinical behavior was benign (51). The US features of struma ovarii are nonspecific, but a heterogeneous, predominantly solid mass may be seen. US demonstrates a complex appearance with multiple cystic and solid areas, findings that reflect the gross pathologic appearance of the tumor. MR imaging findings may be more characteristic: The cystic spaces demonstrate both high and low signal intensity on T1- and T2-weighted images (Fig 10) (2,52). Some of the cystic spaces may demonstrate low signal intensity on both T1- and T2-weighted images due to the thick, gelatinous colloid of the struma (2,53,54). No fat is evident in these lesions.

Carcinoid Tumors

Carcinoid tumors of the ovary are uncommon. They may be insular (islet tumors), trabecular, or mucinous. All types are frequently associated with a mature cystic teratoma or mucinous tumor (14, 51). At gross pathologic examination, ovarian carcinoid tumors are solid (14,49).

Unlike most mature cystic teratomas, ovarian carcinoid tumors usually occur in postmenopausal women (14). Although they are considered to have a potential for malignancy, most of these tumors have a relatively benign clinical course, with metastases being uncommon. Secretory granules are seen within the tumor cells, and immunocytochemical analysis demonstrates serotonin and hormonal peptides, which are typically present in carcinoid tumors (14,51). Carcinoid syndrome is uncommon.

The imaging appearance of ovarian carcinoid tumors is not well described. Because these are solid tumors, they would be expected to be indistinguishable from solid malignancies, although necrosis is less common in the former. Mucinous carcinoid tumors have higher signal intensity on T2-weighted MR images than do most solid tumors because they contain high-signal-intensity mucin (Fig 11).

Neural Tumors

Other types of monodermal teratomas have been described. Monodermal teratomas with neuroectodermal differentiation can form benign, ependymoma-like tumors or primitive neuroectodermal tumors (51). The latter are very aggressive tumors with a poor prognosis.

Conclusions

The most common types of teratoma, mature and immature teratoma, both demonstrate lipid material at CT and MR imaging. This material consists of sebaceous material within the cyst cavity or adipose tissue within the cyst wall or dermoid plug. The morphologic features of the tumors differ in that mature cystic teratomas (dermoid cysts) are predominantly cystic, whereas immature teratomas are predominantly solid with small foci of fat. Struma ovarii and carcinoid tumors are monodermal teratomas and do not demonstrate fat. Struma ovarii has a multilocular appearance with loculations of varying signal intensity on both T1- and T2-weighted MR images.

References

1. Kido A, Togashi K, Konishi I, et al. Dermoid cysts of the ovary with malignant transformation: MR appearance. AJR Am J Roentgenol 1999; 172:445–449.
2. Yamashita Y, Hatanaka Y, Takahashi M, Miyazaki K, Okamura H. Struma ovarii: MR appearances. Abdom Imaging 1997; 22:100–102.
3. Dohke M, Watanabe Y, Takahashi A, et al. Struma ovarii: MR findings. J Comput Assist Tomogr 1997; 21:265–267.
4. Kawakami S, Togashi K, Egawa H, et al. Solid mature teratoma of the ovary: appearances at MR imaging. Comput Med Imaging Graph 1994; 18:203–207.
5. Hatanaka Y, Yamashita Y, Torashima M, Takahashi M. MR appearance of fat distribution in ovarian teratoma: pathologic correlation. Nippon Igaku Hoshasen Gakkai Zasshi 1996; 56:477–481. [Japanese]
6. Comerci JT Jr, Licciardi F, Bergh PA, Gregori C, Breen JL. Mature cystic teratoma: a clinicopathologic evaluation of 517 cases and review of the literature. Obstet Gynecol 1994; 84:22–28.
7. Koonings PP, Campbell K, Mishell DR Jr, Grimes DA. Relative frequency of primary ovarian neoplasms: a 10-year review. Obstet Gynecol 1989; 74: 921–926.
8. Whitecar MP, Turner S, Higby MK. Adnexal masses in pregnancy: a review of 130 cases undergoing surgical management. Am J Obstet Gynecol 1999; 181: 19–24.
9. Brown MF, Hebra A, McGeehin K, Ross AJ III. Ovarian masses in children: a review of 91 cases of malignant and benign masses. J Pediatr Surg 1993; 28:930–933.
10. Linder D, McCaw BK, Hecht F. Parthenogenic origin of benign ovarian teratomas. N Engl J Med 1975; 292:63–66.
11. Caspi B, Appelman Z, Rabinerson D, Zalel Y, Tulandi T, Shoham Z. The growth pattern of ovarian dermoid cysts: a prospective study in premenopausal and postmenopausal women. Fertil Steril 1997; 68: 501–505.
12. Caruso PA, Marsh MR, Minkowitz S, Karten G. An intense clinicopathologic study of 305 teratomas of the ovary. Cancer 1971; 27:343–348.
13. Blackwell WJ, Dockerty MB, Mason JC, Mussey RD. Dermoid cysts of the ovary: their clinical and pathological significance. Am J Obstet Gynecol 1946; 51: 151–172.
14. Talerman A. Germ cell tumors of the ovary. In: Kurman RJ, ed. Blaustein's pathology of the female genital tract. 4th ed. New York, NY: Springer-Verlag, 1994; 849–914.
15. Matz MH. Benign cystic teratomas of the ovary. Obstet Gynecol Surv 1961; 16:591–605.
16. Quinn SF, Erickson S, Black WC. Cystic ovarian teratomas: the sonographic appearance of the dermoid plug. Radiology 1985; 155:477–478.
17. Patel MD, Feldstein VA, Lipson SD, Chen DC, Filly RA. Cystic teratomas of the ovary: diagnostic value of sonography. AJR Am J Roentgenol 1998; 171:1061–1065.
18. Dodd GD, Budzik RF. Lipomatous tumors of the pelvis in women: spectrum of imaging findings. AJR Am J Roentgenol 1990; 155:317–322.
19. Sheth S, Fishman EK, Buck JL, Hamper UM, Sanders RC. The variable sonographic appearances of ovarian teratomas: correlation with CT. AJR Am J Roentgenol 1988; 151:331–334.

20. Mais V, Guerriero S, Ajossa S, Angiolucci M, Paoletti AM, Melis GB. Transvaginal ultrasonography in the diagnosis of cystic teratoma. Obstet Gynecol 1995; 85:48–52.
21. Hertzberg BS, Kliewer MA. Sonography of benign cystic teratoma of the ovary: pitfalls in diagnosis. AJR Am J Roentgenol 1996; 167:1127–1133.
22. Caspi B, Appelman Z, Rabinerson D, Elchalal U, Zalel Y, Katz Z. Pathognomonic echo patterns of benign cystic teratomas of the ovary: classification, incidence and accuracy rate of sonographic diagnosis. Ultrasound Obstet Gynecol 1996; 7:275–279.
23. Guerriero S, Mallarini G, Ajossa S, et al. Transvaginal ultrasound and computed tomography combined with clinical parameters and CA-125 determinations in the differential diagnosis of persistent ovarian cysts in premenopausal women. Ultrasound Obstetr Gynecol 1997; 9:339–343.
24. Occhipinti KA, Frankel SD, Hricak H. The ovary: computed tomography and magnetic resonance imaging. Radiol Clin North Am 1993; 31:1115–1132.
25. Buy JN, Ghossain MA, Moss AA, et al. Cystic teratoma of the ovary: CT detection. Radiology 1989; 171:697–701.
26. Togashi K, Nishimura K, Itoh K, et al. Ovarian cystic teratomas: MR imaging. Radiology 1987; 162:669–673.
27. Guinet C, Buy JN, Ghossain MA, et al. Fat suppression techniques in MR imaging of mature ovarian teratomas: comparison with CT. Eur J Radiol 1993; 17:117–121.
28. Imaoka I, Sugimura K, Okizuka H, Iwanari O, Kitao M, Ishida T. Ovarian cystic teratomas: value of chemical fat saturation magnetic resonance imaging. Br J Radiol 1993; 66:994–997.
29. Kier R, Smith RC, McCarthy SM. Value of lipid- and water-suppression MR images in distinguishing between blood and lipid within ovarian masses. AJR Am J Roentgenol 1992; 158:321–325.
30. Mitchell DG, Outwater EK. Benign gynecologic disease: applications of magnetic resonance imaging. Top Magn Reson Imaging 1995; 7:26–43.
31. Stevens SK, Hricak H, Campos Z. Teratomas versus cystic hemorrhagic adnexal lesions: differentiation with proton-selective fat-saturation MR imaging. Radiology 1993; 186:481–488.
32. Scoutt L, McCarthy S, Lange R, Bourque A, Schwartz P. MR evaluation of clinically suspected adnexal masses. J Comput Assist Tomogr 1994; 18: 609–618.
33. Yamashita Y, Torashima M, Hatanaka Y, et al. Value of phase-shift gradient-echo MR imaging in the differentiation of pelvic lesions with high signal intensity at T1-weighted imaging. Radiology 1994; 191:759–764.
34. Yamashita Y, Hatanaka Y, Torashima M, Takahashi M, Miyazaki K, Okamura H. Mature cystic teratomas of the ovary without fat in the cystic cavity: MR features in 12 cases. AJR Am J Roentgenol 1994; 163: 613–616.
35. Muramatsu Y, Moriyama N, Takayasu K, Nawano S, Yamada T. CT and MR imaging of cystic ovarian teratoma with intracystic fat balls. J Comput Assist Tomogr 1991; 15:528–529.
36. Kimura I, Togashi K, Kawakami S, Takakura K, Mori T, Konishi J. Ovarian torsion: CT and MR imaging appearances. Radiology 1994; 190:337–341.
37. Kawakami K, Murata K, Kawaguchi N, et al. Hemorrhagic infarction of the diseased ovary: a common MR finding in two cases. Magn Reson Imaging 1993; 11:595–597.
38. Wisniewski M, Deppisch LM. Solid teratomas of the ovary. Cancer 1973; 32:440–446.
39. Malkasian GD, Symmonds GD, Dockerty MB. Malignant ovarian teratomas. Obstet Gynecol 1965; 25: 810–814.
40. Heifetz SA, Cushing B, Giller R, et al. Immature teratomas in children: pathologic considerations: a report from the combined Pediatric Oncology Group/ Children's Cancer Group. Am J Surg Pathol 1998; 22:1115–1124.
41. Cushing B, Giller R, Ablin A, et al. Surgical resection alone is effective treatment for ovarian immature teratoma in children and adolescents: a report of the pediatric oncology group and the children's cancer group. Am J Obstet Gynecol 1999; 181:353–358.
42. Yanai-Inbar I, Scully RE. Relation of ovarian dermoid cysts and immature teratomas: an analysis of 350 cases of immature teratoma and 10 cases of dermoid cyst with microscopic foci of immature tissue. Int J Gynecol Pathol 1987; 6:203–212.
43. Moskovic E, Jobling T, Fisher C, Wiltshaw E, Parsons C. Retroconversion of immature teratoma of the ovary: CT appearances. Clin Radiol 1991; 43:402–408.
44. Caldas C, Sitzmann J, Trimble CL, McGuire WP III. Synchronous mature teratomas of the ovary and liver: a case presenting 11 years following chemotherapy for immature teratoma. Gynecol Oncol 1992; 47:385–390.
45. Sutton CL, McKinney CD, Jones JE, Gay SB. Ovarian masses revisited: radiologic and pathologic correlation. RadioGraphics 1992; 12:853–877.
46. Brammer HM III, Buck JL, Hayes WS, Sheth S, Tavassoli FA. From the archives of the AFIP. Malignant germ cell tumors of the ovary: radiologic-pathologic correlation. RadioGraphics 1990; 10:715–724.
47. Bazot M, Cortez A, Sananes S, Boudghene F, Uzan S, Bigot JM. Imaging of dermoid cysts with foci of immature tissue. J Comput Assist Tomogr 1999; 23: 703–706.
48. Outwater EK, Dunton CJ. Imaging of the ovary and adnexa: clinical issues and applications of MR imaging. Radiology 1995; 194:1–18.
49. Scully RE. Tumors of the ovary and maldeveloped gonads. In: Hartmann WH, ed. Atlas of tumor pathology. Vol 2. Washington, DC: Armed Forces Institute of Pathology, 1979; 252–253.
50. Clement PB, Young RH, Scully RE. Clinical syndromes associated with tumors of the female genital tract. Semin Diagn Pathol 1991; 8:204–233.
51. Young RH. New and unusual aspects of ovarian germ cell tumors. Am J Surg Pathol 1993; 17:1210–1224.
52. Matsumoto F, Yoshioka H, Hamada T, Ishida O, Noda K. Struma ovarii: CT and MR findings. J Comput Assist Tomogr 1990; 14:310–312.
53. Joja I, Asakawa T, Mitsumori A, et al. Struma ovarii: appearance on MR images. Abdom Imaging 1998; 23:652–656.
54. Matsuki M, Kaji Y, Matsuo M, Kobashi Y. Struma ovarii: MRI findings. Br J Radiol 2000; 73:87–90.

This article meets the criteria for 1.0 credit hour in category 1 of the AMA Physician's Recognition Award. To obtain credit, see accompanying test at http://www.rsna.org/education/rg_cme.html.